Magnetic Resonance Imaging 58 (2019) 24–31

Contents lists available at ScienceDirect

Magnetic Resonance Imaging

journal homepage: www.elsevier.com/locate/mri

Original contribution

Using functional magnetic resonance imaging to evaluate an acute allograft rejection model in rats

Song Zeng[a,b,1], Lu Liang[c,1], Qiang Zhang[a,b], Yue Xu[a,b], Hao Tang[a,b], Zijian Zhang[a,b], Xiaodong Zhang[a,b], Tao Jiang[c,**], Xiaopeng Hu[a,b,*]

[a] Department of Urology, Beijing Chao-Yang Hospital, Capital Medical University, Beijing, China
[b] Institute of Urology, Capital Medical University, Beijing, China
[c] Department of Radiology, Beijing Chao-Yang Hospital, Capital Medical University, Beijing, China

ARTICLE INFO

Keywords:
Functional MRI
Intravoxel incoherent motion
Blood oxygen level-dependent
Kidney transplantation
Rejection

ABSTRACT

Purpose: To assess the longitudinal changes of allograft pathophysiology by intravoxel incoherent motion (IVIM) and blood oxygen level-dependent (BOLD) MRI in a rat model of acute renal allograft rejection.

Materials and methods: Acute rejection (AR) was induced by transplantation of Dark Agouti donor kidneys into Lewis recipients (n = 18). A Lewis-Lewis rat syngeneically transplanted (sTX) model served as the control (n = 6). Acute tubular necrosis (n = 6) and acute calcineurin inhibitor toxicity (n = 6) groups were established using Lewis rats. MRI was performed on postoperative day (POD) 1, 4 and 7 in the allogeneically transplanted (aTX) group and on POD4 in the other groups. Histological evaluation and PCR were performed.

Results: After the allogenic transplantation, all MRI parameters of allograft further decreased until POD7, and the D and ADC values in the cortex were significantly lower than that in the sTX group (1.03 ± 0.09 vs 1.52 ± 0.09 × 10^{-3} mm^2/s, P_{adj} < 0.05; 1.21 ± 0.03 vs 1.78 ± 0.07 × 10^{-3} mm^2/s, P_{adj} < 0.05). The D*, f and R2* values of the aTX group in the cortex and medulla were significantly lower than those in the sTX group on POD7 (cortex, D*: 25.60 ± 4.78 vs 69.32 ± 9.79 × 10^{-3} mm^2/s, P_{adj} < 0.05; f: 7.84 ± 1.83 vs 20.34 ± 3.08%, P_{adj} < 0.05; R2*: 16.61 ± 4.18 vs 31.48 ± 6.43 1/s, P_{adj} < 0.05; medulla, D*: 13.59 ± 6.08 vs 62.75 ± 9.20 × 10^{-3} mm^2/s, P_{adj} < 0.05; f: 7.46 ± 1.62 vs 14.68 ± 2.05%, P_{adj} < 0.05; R2*: 21.59 ± 3.45 vs 39.53 ± 4.34 1/s, P_{adj} < 0.05). AR grafts presented serve interstitial inflammation, tubulitis and infiltration of T-lymphocytes and macrophages. The MRI parameters, including D, ADC, D*, f and R2*, were significantly correlated with the histological changes, cell infiltration and inflammatory cytokine mRNA levels.

Conclusions: IVIM coupled with BOLD MRI allows longitudinal assessment of allograft diffusion, perfusion and oxygen consumption impairment caused by acute renal allograft rejection in rat model.

1. Introduction

Acute renal allograft rejection is the leading cause of allograft damage and low long-term graft survival [1]. Currently, allograft biopsy is the gold standard for diagnosing acute rejection (AR) and for differentiation from other causes of renal dysfunction. However, as an invasive method, biopsies are not suitable for repeated and dynamic monitoring. Therefore, noninvasive and comprehensive monitoring of allograft pathophysiology would be desirable.

Functional magnetic resonance imaging (fMRI) can show pathophysiological changes in renal allografts without invasiveness in addition to morphological changes [2]. In particular, diffusion-weighted imaging (DWI) and blood oxygen level-dependent (BOLD) MRI have been used to monitor the function of renal allografts in clinical study and experimental study in small animals [3–5]. The apparent diffusion coefficient (ADC), a quantitative parameter derived from DWI, reflects the microscopic motion of water molecules in tissue [6]. BOLD can evaluate renal oxygenation by means of the R2* value (=1/T2*) which is inversely correlated with pO_2 and positively correlated with deoxyhemoglobin [7]. Le Bihan et al. indicated that microscopic motion in tissue includes microcirculation perfusion and the diffusion of water molecules [8]. Intravoxel incoherent motion (IVIM)

* Correspondence to: X. Hu, Department of Urology, Beijing Chao-Yang Hospital, Capital Medical University, NO.8 GongTi South Road, 100020 Beijing, China.
** Correspondence to: T. Jiang, Department of Radiology, Beijing Chao-Yang Hospital, Capital Medical University, NO.8 GongTi South Road, 100020 Beijing, China
E-mail addresses: jiangt8166@hotmail.com (T. Jiang), xiaopeng_hu@sina.com (X. Hu).
[1] Song Zeng and Lu Liang contributed equally to this work.

https://doi.org/10.1016/j.mri.2019.01.006
Received 28 August 2018; Received in revised form 3 December 2018; Accepted 6 January 2019

can quantitatively assess the renal fluid loading and microvascular dynamics via the parameters, including the pseudo-diffusion coefficient (D*), pure diffusion coefficient (D) and volume fraction (f).

Normal kidneys are characterized by the active diffusion of water molecules and rich blood circulation, whereas AR is characterized by endothelial inflammation, interstitial inflammation, edema and the swelling of small renal arteries. These characteristics can result in changes in the diffusion of water molecules and microcirculation; all of these issues constitute the basis of this study.

The aim of this study was to investigate the value of IVIM and BOLD MRI for evaluating the renal pathophysiology in rat models of AR. Moreover, we intended to compare fMRI parameters with histopathology and real time-polymerase chain reaction (PCR) data. Furthermore, because the cause of delayed graft function during the early stage after renal transplantation needs to be determined, we evaluated whether IVIM can be used to differentiate AR, the acute tubular necrosis (ATN) occurring after ischemia-reperfusion injury (IRI) and the acute calcineurin inhibitor toxicity caused by cyclosporin A (CSA).

2. Materials and methods

2.1. Experimental animals and reagents

This study was conducted with the approval of the animal protection committee of the Capital Medical University (approval: AEEI-2017-010). Animals were cared in accordance with the National Institutes of Health guidelines. Eight- to 12-week-old, inbred male Dark Agouti (DA) and Lewis (LEW) rats weighing 200 to 250 g were provided by Vital River (Beijing, China; National Experimental Animal Seed Center). Rats were reared under the conditions as follows: temperature, 22 ± 1 °C; relative humidity, 55 ± 5%; and free access to water and normal diet under 12/12-hour day-night cycle. Any visible side effects or unusual behavior of the animals were monitored on a daily basis.

The hematoxylin-eosin (HE) staining kit, periodic acid-Schiff (PAS) staining reagent and HRP-Polymer IHC kit were purchased from TechLab (Beijing, China). The antirat CD3 and CD68 antibodies were purchased from Abcam (Cambridge, UK). The SYBR qPCR regent was purchased from Invitrogen (American).

2.2. Animal model establishment

Four animal models were designed in this study (Fig. 1).

Kidney transplantation was conducted in twenty-five rats by a surgeon with > 5-year experience in small animal microsurgery. Before the surgery, rats were fasted for 24 h without water deprivation. Isoflurane mixed with oxygen was used for inhalation anesthesia. General anesthesia was induced by 3% and maintained by 1.5% isoflurane. Orthotopic kidney transplantation was performed, as described previously in detail [9]. Briefly, donor left kidney was perfused with 3–5 ml ice saline mixed with heparin until the color of kidney turned white. Then the kidney was flushed and persevered in cold saline at 4 °C before reperfusion. The recipients underwent left nephrectomy but with 2 mm renal artery and vein preserved. Then the kidney graft was transplanted into the left renal fossa of the recipient. The artery of the allograft was anastomosed to the recipient's renal artery using end-to-end anastomosis, and the renal vein was anastomosed with cuff. The kidney transplantation was completed with a ureteroureterostomy. Maintenance of normal renal function was ensured by the remaining unaffected right kidney. Consequently, in case of AR, rats could survive through POD7 to complete the experiment. Cold ischemia time was 45 min, and warm ischemia time was 1 min. The total operation time was about 90 min. One rat was excluded due to the left renal cyst. In addition, rats with early postsurgical complication such as graft thrombosis, bleeding, or urinary leakage, were excluded.

AR was induced by allogeneic transplantation of DA allografts into LEW-recipients [10], thereby establishing an allogeneically transplanted (aTX) model (n = 18). A LEW-LEW rat syngeneically transplanted (sTX) model served as the control (n = 6). The methods for establishing IRI and CSA models have been validated [11,12]. After inhalation anesthesia, a microvascular clip was used to clamp the left renal artery of LEW rats for 45 min to establish an IRI model (n = 6). Calcineurin inhibitor toxicity was induced in LEW rats by injecting CSA (50 mg/kg/BW i.p.) for 2 days (n = 6).

In the pilot experiment, the function of the sTX kidneys remained normal with no histological changes, which was consistent with the findings in other studies [13]. The typical IRI and CSA damage was present on postoperative day (POD) 4, as well as rejection. However, the aTX graft was still function until the necrosis occurred on POD 5–6, ultimately leading to death around POD 7. Based on these findings, six rats were imaged longitudinally on POD 1, 4 and 7 after allogeneic transplantation, and four rats randomly chosen from the remaining twelve aTX rats were sacrificed for histological studies at each time point. In addition, fMRI was conducted on POD 4 for the other groups, including sTX, IRI and CSA group. No rats had been excluded during the experiment.

2.3. MRI protocol

All experiments were performed using a 3.0-T imager (MAGNETOM Prisma System; Siemens Medical Solutions, Erlangen, Germany) with a 64-channel phased array coil. Before the MRI, the rats were fasted for 12 h with water deprivation for 4 h to avoid the influence of intestinal peristalsis and gas. In addition, 1 mg glucagon (Glucagon G Novo, Eisai, Tokyo, Japan) was intramuscularly administered before imaging to prevent artifacts from bowel peristalsis. During the MRI, the abdomen was squeezed using cotton to reduce breathing artifacts. The rats were anesthetized with 3% isoflurane and maintained with 1.5% isoflurane. The depth of anesthesia was monitored using the respiratory rate. Maintenance of the body temperature of the rats in the scanner was ensured by the constant room temperature at 37 °C.

The imaging sequence included T1-weighted images, T2-weighted images, BOLD MRI and IVIM DWI MRI. Eight b values (0, 50, 100, 150, 200, 400, 800 and 1000 s/mm^2) were applied in IVIM DWI. The sequence parameters are listed in Table 1.

A Siemens Syngo.via image processing workstation was used. The DWI and BOLD raw data were sent to the workstation to determine ADC and R2*, and the MITK-diffusion software (downloadable at http://www.mitk.org/) was then used for the image processing of the IVIM raw data to obtain D, D* and f. Regions of interest, covering the whole renal cortex and medulla, including the upper, middle and lower renal poles (region size ~ 1 to 2 mm^2, including at least 5 pixels), were placed manually by a blinded radiologist with > 10-year experience (Fig. 2a). The same radiologist performed the image processing and data reading for each group. The relative signal change (%) was calculated by comparing the parameters of different groups with those of the sTX group.

2.4. Histological examination

The rats were sacrificed by intraperitoneal injection with lethal doses of 10% chloral hydrate. Besides, kidneys were perfused with cold saline until the color of kidney turned white. Paraffin-embedded renal specimens were serially sectioned (3 μm) and stained with HE and PAS reaction. Two blinded independent pathologists determined the histopathological score according to the criteria of Banff 2013 [14].

In addition, immunohistochemistry was performed for CD3-positive T-lymphocyte (anti-CD3 antibody, 1:100) and CD68-positive macrophage (anti-CD68 antibody, 1:500). Twelve high-power fields were selected for each kidney. ImageJ software with the ITCN plugin (downloadable at http://rsb.info.nih.gov/ij) was used to determine the number of positive cells within a 350 × 250 μm^2 area in each field, and

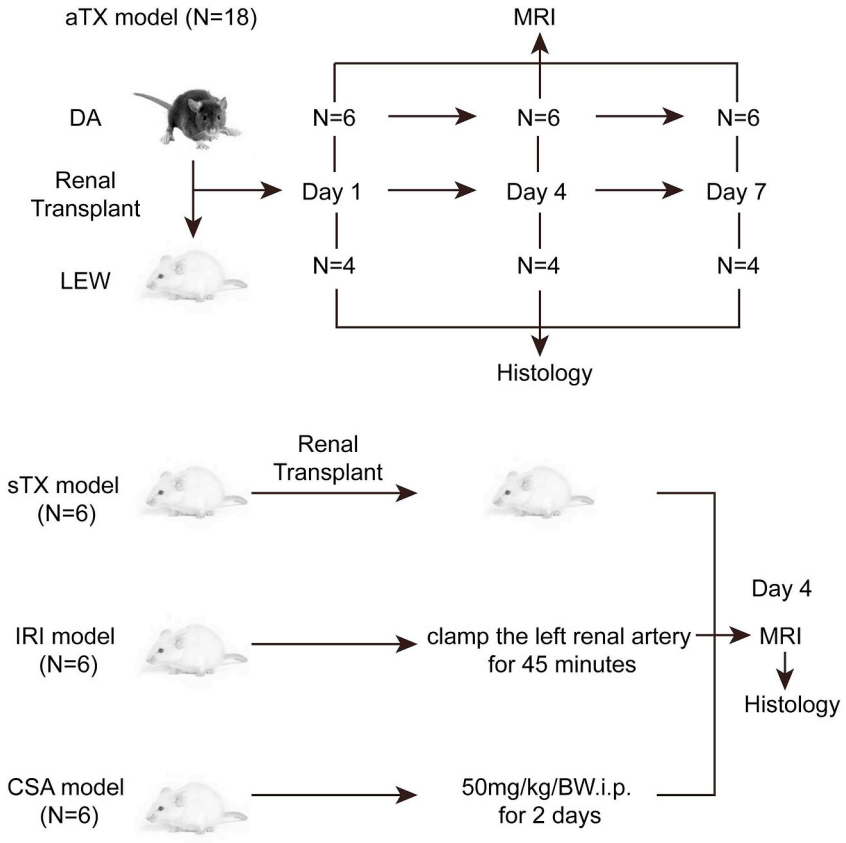

Fig. 1. Study design, group designations, and sample size. The protocol is shown for experiments in the aTX, sTX, IRI and CSA model. aTX = allogeneically transplanted, sTX = syngeneically transplanted, IRI = ischemia-reperfusion injury, CSA = cyclosporin A toxicity.

Table 1
Sequence parameters.

	T1 Turbo Spin Echo	T2 Turbo Spin Echo	BOLD	IVIM DWI
Slice orientation	Coronal	Coronal	Axial	Axial
Respiratory triggering	Yes	Yes	Yes	Yes
FOV, cm^2	12 × 12	12 × 12	12 × 10	12 × 10
Slice thickness, mm	2	2	2	3
Slice gap, mm	0.2	0.2	0.2	0.1
TR, ms	650	3460	229	2100
TE, ms	10	35	3.75, 7.85	44, 69
Matrix	256 × 256	256 × 256	288 × 202	120 × 84
NEX	4	4	4	1
Acquisition time, minute	4m10s	5m41s	6m55s	16m22s

the mean value was used for subsequent analysis [15].

2.5. Real-time PCR

Total RNA was extracted from the renal tissue to synthesize cDNA via reverse transcription. The primers used in this study are listed in Table 2. An ABI 7500 real-time PCR system (Applied Biosystems, Foster City, CA, USA) was used for the PCR. Target mRNA levels were normalized against GAPDH standards and calculated using the $2^{-\Delta\Delta Ct}$ method.

2.6. Statistical analysis

Statistical analysis was performed using SPSS 24.0 (Chicago, IL, USA) and GraphPad Prism 6.0 (San Diego, CA, USA). Data are presented as the mean ± standard deviation (SD). Inter-group differences were compared using the Kruskal-Wallis H test. Only if K test was significant, the p value for pairwise comparisons was computed with the Mann-Whitney U test with Bonferroni correction [16]. Spearman correlation coefficients were used for linear correlations. $P < 0.05$ was considered statistically significant.

3. Results

3.1. Renal diffusion changes

The diffusion parameters D and ADC are shown in Fig. 3 and Table 3. The rats with AR had a progressive reduction in D and ADC in the cortex by 3.2% and 7.3%, respectively, compared with that in the sTX group on POD1, and the minimum D (decreased by 32.2%, $P_{adj} < 0.01$) and ADC (decreased by 32.0%, $P_{adj} < 0.01$) values occurred on POD7 (Fig. 3a). A similar pattern was observed in the medulla of the aTX group, whereas only the ADC values were significantly lower than that in the sTX group on POD7 (1.25 ± 0.04 vs 1.43 ± 0.03 × 10^{-3} mm^2/s, $P_{adj} < 0.05$; Fig. 3b).

3.2. Renal perfusion and oxygenation changes

The D*, f and R2* values are summarized in Table 4. The D*, f and R2* values of the aTX group in the cortex and medulla were lower than those in the sTX group during the early stage of AR, but the difference was significantly only on POD7 (cortex, D*: 25.60 ± 4.78 vs 69.32 ± 9.79 × 10^{-3} mm^2/s, $P_{adj} < 0.05$; f: 7.84 ± 1.83 vs 20.34 ± 3.08%, $P_{adj} < 0.05$; R2*: 16.61 ± 4.18 vs 31.48 ± 6.43 1/s, $P_{adj} < 0.05$; medulla, D*: 13.59 ± 6.08 vs 62.75 ± 9.20 × 10^{-3} mm^2/s, $P_{adj} < 0.05$; f: 7.46 ± 1.62 vs 14.68 ± 2.05%, $P_{adj} < 0.05$; R2*: 21.59 ± 3.45 vs 39.53 ± 4.34 1/

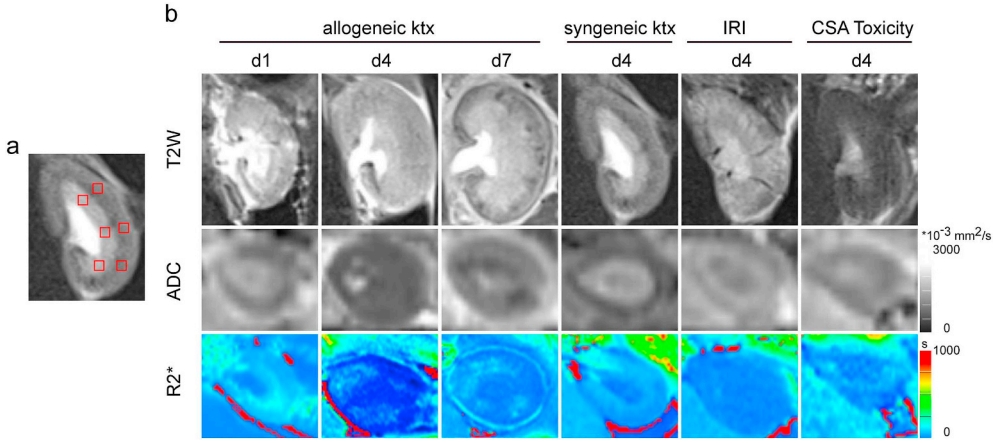

Fig. 2. MRI images of allografts and injured kidneys in different models. (A)View of T2W image of the allograft in the sTX model showing the location of six regions of interest. (B)MRI parameter maps of T2W, ADC and R2* are shown.

s, $P_{adj} < 0.05$). By POD7, the D* value was significantly lower in the cortex of the aTX group than in the IRI and CSA groups (25.60 ± 4.78 vs 64.74 ± 15.27 vs 62.59 ± 8.13 × 10^{-3} mm^2/s, $P_{adj} < 0.05$), and the f value in the medulla also differed significantly by POD7 (7.46 ± 1.62 vs 13.42 ± 2.49 vs 13.29 ± 1.56%, $P_{adj} < 0.05$). A significant difference was observed for R2* in both the cortex and medulla on POD7 between the aTX group and the other groups. In addition, the R2* values were higher in the CSA group than in the sTX group, but the difference was not statistically significant (Fig. 3c, d).

3.3. Histology

Only the allografts of the aTX group presented AR features, including interstitial inflammation and tubulitis (Fig. 4a). Moreover, the severity increased progressively over time, and the Banff scoring indicated the same trend (Fig. 4b). In addition, the CD3 and CD68 immunohistologic staining of the tissues showed significant infiltration of CD3-positive T-lymphocytes and CD68-positive macrophages in allografts undergoing AR starting on POD1 with a further increase through POD7, while this change was absent in the other groups (Fig. 4a, c). However, other changes related to renal damage, such as vacuolization of tubular epithelial cells, were observed in the IRI and CSA groups (Fig. 4a).

3.4. Real-time PCR

The mRNA levels of CD3 and inflammatory cytokines, such as IFN-γ, IL-6 and IL-17, were significantly upregulated only in the allografts of the aTX group, and the difference was more pronounced with time after operation, which was consistent with the histological findings (Fig. 5).

3.5. Correlation of MRI parameters with histology and mRNA expression

Spearman correlation tests were performed to analyze the correlation between the MRI parameters, histological findings and mRNA level in the whole aTX allografts (Table 5). All of the MRI parameters negatively correlated with the Banff scoring, the quantity of infiltrating CD3-positive T-lymphocytes and CD68-positive macrophages, and the mRNA levels of CD3, IFN-γ, IL-6 and IL-17.

4. Discussion

This experimental study showed that fMRI with IVIM and BOLD could be an effective, noninvasive tool for detection and monitoring the change of pathophysiology of the graft with AR, including diffusion and perfusion impairment, a decrease in oxygen consumption and an increased oxygen concentration. These changes were closely related to evidence of inflammation, the quantity of infiltrating cells and the mRNA levels of CD3 and inflammatory cytokines.

In this study, ADC was significantly lower in the aTX group than in the sTX group, indicating a decrease in the diffusion of water molecules in the aTX group, which was consistent with the findings of other studies [17,18]. This was believed to be related to the rejection and tubular necrosis in the grafts. During AR, it is difficult for water molecules to move in cells because of the cell edema, which restricts the diffusion of water molecules [19]. Moreover, the cortex D and ADC values were lower in the IRI and CSA groups than in the sTX group, which may be related to tubular necrosis.

In addition to providing diffusivity information, IVIM yields the parameters D* and f. D* was showed to be sensitive to vascular blood [20], whereas f reflects the ratio of the fluid in the vascular and renal tubules to the total fluid in the renal system [21]. Our study showed that the D* and f values were significantly decreased in the aTX group, suggesting that the microcirculation was significantly lower in the aTX group than in the sTX group; this finding was related to the infiltration of immune cells, the edema of small vascular walls and the endothelial swelling that resulted in a lower blood flow in local microcirculation [22].

Since the renal cortex was supplied by abundant blood vessels, it received up to 90% of total renal blood flow in normal conditions, with

Table 2
List of primers used for RT-PCR.

Gene	Forward sequence	Reverse sequence
CD3	TTCAAGATAGAAGTGGTTGAATATG	CACCTCCTTCGCCAGCTCC
IFN-γ	GCTAGATTCTGGTGACAGCTGGTG	CACCAGCTGTCACCAGAATCTAGC
IL-6	CTTCCAGCCAGTTGCCTTCT	GACAGCATTGGAAGTTGGGG
IL-17	ACATGTAAGGCAGCGGTACT	GCTCAGAGTCCAGGGTGAAG
GAPDH	CATCAACGACCCCTTCATTGAC	ACTCCACGACATACTCAGCACC

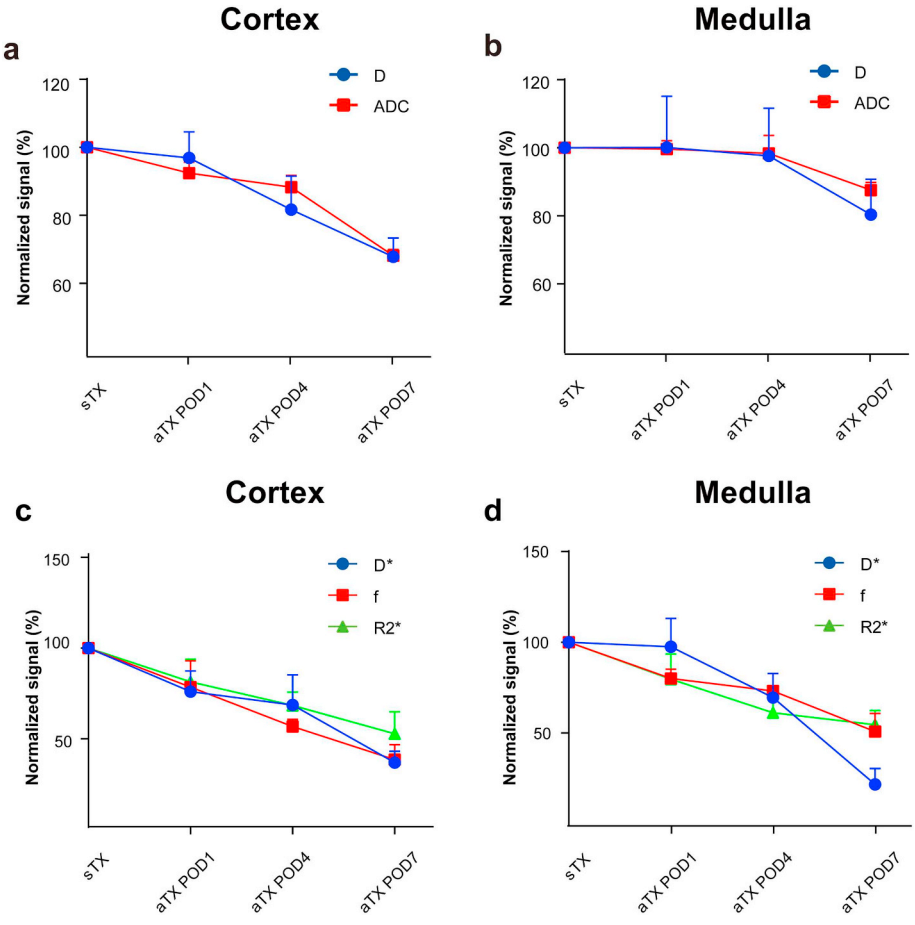

Fig. 3. Changes in the MRI parameters. (A)The cortex D (blue line) and ADC values (red line) at different time points in different groups. (B)Medulla D and ADC values at different time points in different groups. (C)The cortex medulla D* (blue line), f (red line) and R2* values (green line) at different time points in different groups. (D)Medulla D*, f and R2* values at different time points in different groups. (For interpretation of the references to color in this figure legend, the reader is referred to the web version of this article.)

Table 3
The mean D and ADC values ($\times 10^{-3}$ mm^2/s) of kidney in different groups.

Group	Cortex				Medulla			
	D	P_{adj}	ADC	P_{adj}	D	P_{adj}	ADC	P_{adj}
sTX	1.52 ± 0.09	–	1.78 ± 0.07	–	1.24 ± 0.16	–	1.43 ± 0.03	–
aTX POD1	1.47 ± 0.13	1.000	1.65 ± 0.06	1.000	1.24 ± 0.21	1.000	1.42 ± 0.04	1.000
aTX POD4	1.24 ± 0.16	0.560	1.57 ± 0.07	0.937	1.21 ± 0.19	1.000	1.41 ± 0.08	1.000
aTX POD7	1.03 ± 0.09*	0.001	1.21 ± 0.03*	< 0.001	1.00 ± 0.14	0.274	1.25 ± 0.04*	0.027
IRI	1.15 ± 0.07	0.072	1.38 ± 0.04*	0.001	1.25 ± 0.15	1.000	1.41 ± 0.04	1.000
CSA	1.14 ± 0.10	0.051	1.48 ± 0.04	0.092	1.17 ± 0.16	1.000	1.45 ± 0.10	1.000

Note. Kruskal-Wallis H test and Mann-Whitney *U* test for further pairwise comparisons.
sTX, syngeneically transplanted; aTX, allogeneically transplanted; IRI, ischemia-reperfusion injury; CSA, cyclosporin A toxicity.
* Statistical significance compared with the sTX group. $P_{adj} < 0.05$.

Table 4
The mean D_* ($\times 10^{-3}$ mm^2/s), f (%) and $R2_*$ (1/s) values of kidney in different groups.

Group	Cortex						Medulla					
	D_*	$_*P_{adj}$	f	$_*P_{adj}$	$R2_*$	$_*P_{adj}$	D_*	$_*P_{adj}$	f	$_*P_{adj}$	$R2_*$	$_*P_{adj}$
sTX	69.32 ± 9.79	–	20.34 ± 3.08	–	31.48 ± 6.43	–	62.75 ± 9.20	–	14.68 ± 2.05	–	39.53 ± 4.34	–
aTX POD1	52.73 ± 8.69	0.598	15.99 ± 3.25	1	25.63 ± 4.30	1	61.00 ± 10.74	1	11.75 ± 0.83	0.618	31.49 ± 5.99	1
aTX POD4	47.59 ± 12.66	0.277	11.56 ± 0.89*	0.024	21.55 ± 2.55	0.15	43.65 ± 9.09	0.44	10.74 ± 1.56	0.162	24.21 ± 3.03	0.118
aTX POD7	25.60 ± 4.78*	< 0.001	7.84 ± 1.83*	< 0.001	16.61 ± 4.18*	0.014	13.59 ± 6.08*	0.001	7.46 ± 1.62*	< 0.001	21.59 ± 3.45*	0.029
IRI	64.74 ± 15.27#	1	19.64 ± 2.40#	1	29.78 ± 3.25#	1	52.14 ± 13.04	1	13.42 ± 2.49#	1	41.99 ± 3.87#	1
$^{\#}P_{adj}$	0.018	–	< 0.001	–	0.02	–	0.06	–	0.008	–	0.008	–
CSA	62.59 ± 8.13#	1	15.20 ± 1.70	1	33.08 ± 4.77#	1	43.81 ± 11.11	0.598	13.29 ± 1.56#	1	44.41 ± 3.68#	1
$^{\#}P_{adj}$	0.014	–	0.221	–	0.001	–	0.682	–	0.014	–	0.001	–

Note. Kruskal-Wallis H test and Mann-Whitney U test for further pairwise comparisons.
sTX, syngeneically transplanted; aTX, allogeneically transplanted; IRI, ischemia-reperfusion injury; CSA, cyclosporin A toxicity.
* Statistical significance compared with the sTX group. $P_{adj} < 0.05$.
# Statistical significance compared with the aTX POD7. $P_{adj} < 0.05$.

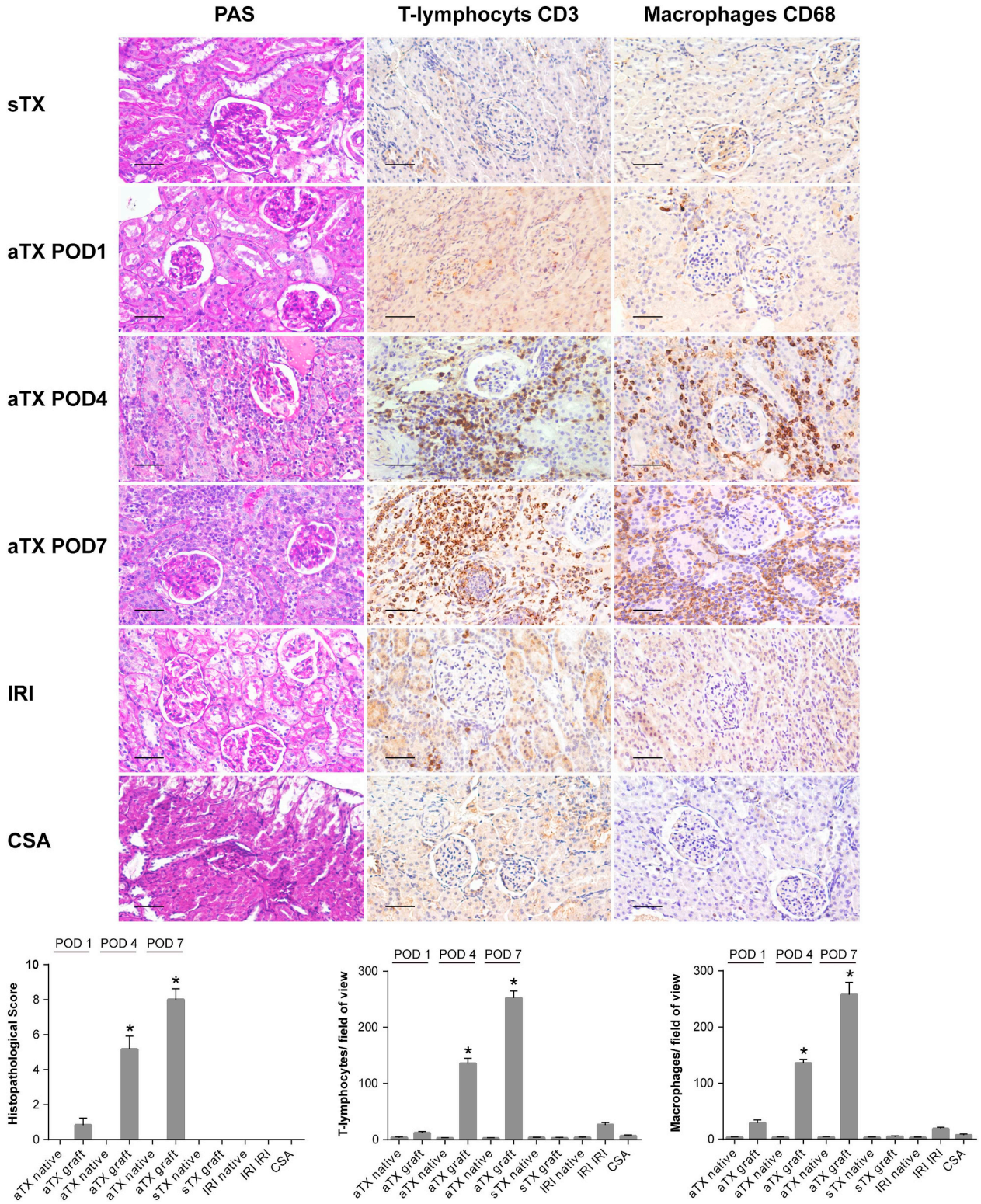

Fig. 4. Renal histological changes in different groups. Histological changes were evaluated on PAS stains (400× magnification) for Banff score, inflammation and vacuolar changes, CD3 stains (400× magnification) for infiltration of T-lymphocytes, and CD68 stains (400× magnification) for infiltration of macrophages. Acute rejection was characterized by interstitial and tubular inflammation, and injured kidneys in the IRI and CSA group presented vacuolar changes in the renal tubular epithelial cells. The morphological changes significantly worsened by POD7 relative to POD1. Scale bar: 50 μm, POD = postoperative day, aTX = allogeneically transplanted, sTX = syngeneically transplanted, IRI = ischemia-reperfusion injury, CSA = cyclosporin A toxicity.

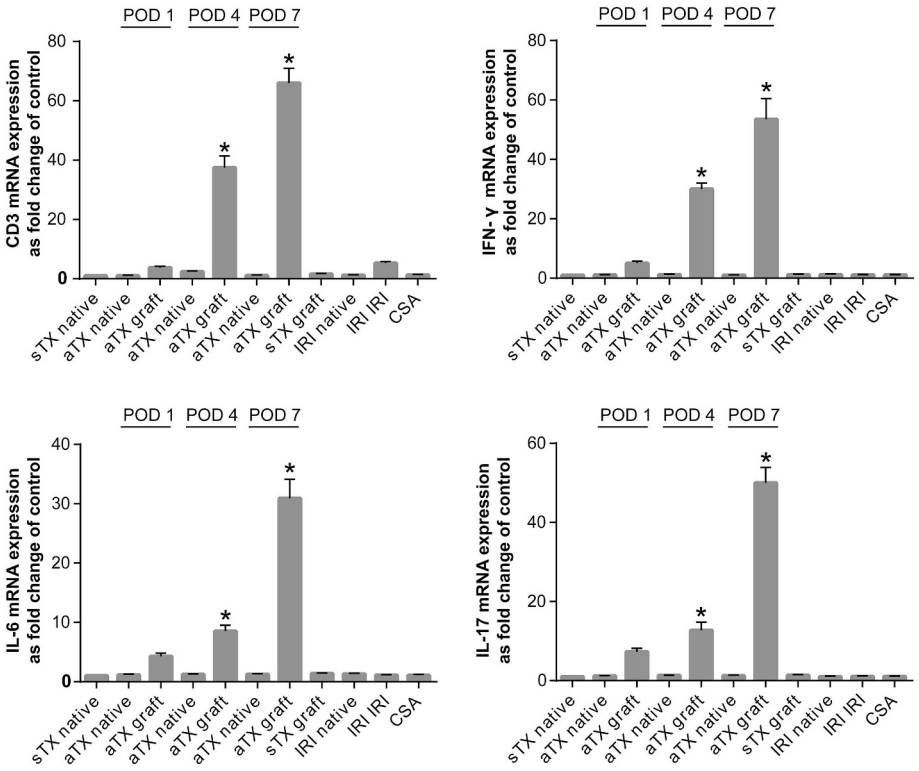

Fig. 5. The mRNA expression of CD3 and inflammatory cytokines in different groups. The mRNA level of CD3 was significantly higher in the renal allograft of the aTX group compared with all other controls by POD 4 ($P_{adj} < 0.05$). mRNA expression of IL-6, IL-17 and IFN-γ was significantly upregulated in renal allografts starting on POD4, compared with other control groups ($P_{adj} < 0.05$). POD = postoperative day, aTX = allogeneically transplanted, sTX = syngeneically transplanted, IRI = ischemia-reperfusion injury, CSA = cyclosporin A toxicity. Significant differences are indicated: $^{*}P_{adj} < 0.05$.

Table 5
Correlation of MRI parameters with histology and mRNA expression.

MRI parameter	D	ADC	D*	f	R2*
Banff score	$r = -0.67$, $P = 0.002$	$r = -0.77$, $P < 0.001$	$r = -0.85$, $P < 0.001$	$r = -0.90$, $P < 0.001$	$r = -0.71$, $P = 0.001$
T-cells	$r = -0.65$, $P = 0.003$	r = −0.72, $P = 0.001$	$r = -0.89$, $P < 0.001$	$r = -0.86$, $P < 0.001$	$r = -0.72$, $P = 0.001$
Macrophages	r = −0.67, $P = 0.002$	$r = -0.76$, $P < 0.001$	r = −0.89, $P < 0.001$	$r = -0.82$, $P < 0.001$	$r = -0.55$, $P = 0.019$
CD3 mRNA	$r = -0.64$, $P = 0.004$	$r = -0.79$, $P < 0.001$	$r = -0.87$, $P < 0.001$	r = −0.86, $P < 0.001$	$r = -0.62$, $P = 0.006$
IFN-γ mRNA	$r = -0.63$, $P = 0.005$	$r = -0.73$, $P = 0.001$	r = −0.89, $P < 0.001$	r = −0.86, $P < 0.001$	$r = -0.75$, $P < 0.001$
IL-6 mRNA	$r = -0.71$. $P = 0.001$	r = −0.79, $P < 0.001$	r = −0.90, $P < 0.001$	r = −0.85, $P < 0.001$	$r = -0.69$, $P = 0.002$
IL-17 mRNA	r = −0.63, $P = 0.005$	$r = -0.74$, $P < 0.001$	r = −0.89, $P < 0.001$	r = −0.87, $P < 0.001$	$r = -0.66$, $P = 0.003$

Note. Spearman correlation analysis for the correlations. P value < 0.05 are considered statistically significant.

the unrestricted diffusion of water molecules. Whereas during AR, extensive cellular and interstitial edema oppressed small blood vessels, resulting in higher vascular resistance, significantly lower diffusion and perfusion in the renal cortex [23], and thus showed more pronounced changes in blood flow than the medulla. Moreover, the local inflammatory response, oxidative stress and the release of cytokines caused a cortex-to-medulla shift in renal flow, resulting in a relatively high medullary flow, which would balance the changes caused by AR in the medulla. Overall, the degree of damage is more severe in the cortex than medulla as the result presented.

The cortex and medulla R2* values were significantly lower in the aTX group than all other groups, indicating a higher tissue oxygen concentration in the aTX group, which was consistent with the findings of previous study [24]. This result was probably related to a decrease in the oxygen consumption or a relatively high medullary flow. Our study showed that the cortex and medulla D* and f values were significantly lower in the aTX group, indicating a significant decrease in microcirculation. The significant impairment of renal perfusion in the AR model was confirmed using fMRI with arterial spin labeling in another study [25]. Thus, this finding suggested that the improvements in the renal oxygen concentration were primarily related to a lower oxygen consumption instead of improvements in the blood supply, which was consistent with the findings of previous study [26].

The histological analysis of the aTX group at different time points revealed that over time, the AR-related histological changes worsened, which was corroborated by the changes in the renal diffusion and perfusion parameters in the aTX group. The linear correlation analysis showed that the high Banff scoring, the infiltration of more cells, and the high mRNA levels of CD3, IFN-γ, IL-6 and IL-17 were negatively correlated with the MRI parameters in the aTX allografts, suggesting that IVIM MRI and BOLD MRI may indirectly reflect the progression of AR, which may be related to worsening cell edema, vascular stenosis and decreases in tubular reabsorption.

This study has certain limitations. First, only a small number of rats was used to perform longitudinal MRI examinations, but this number was sufficient to show differences between the aTX and sTX groups by MRI. Systematic longitudinal studies with more rats will be undertaken to proof the value of fMRI for early detection of acute renal rejection. Furthermore, this technique may not be able to distinguish the kidney inflammation that occurs in AR from the allograft inflammation that occurs in the setting of infection (e.g., urosepsis or BK nephropathy). CEST MRI (both exogenous and endogenous) may be more specific to inflammation than IVIM and BOLD [27,28]. Moreover, the native right kidney was preserved, which may impact the perfusion as the blood flow may preferentially be shunted away from the rejecting kidney to the perfectly functioning native kidney. Since unmodified rejection may be more apparent on MRI than the breakthrough AR occurring in immunosuppressed recipients, a group of subclinically immunosuppressed

recipients who subsequently experience AR should be evaluated in further research. Moreover, human studies are needed to confirm the results and to define the cutoff values for the IVIM diffusion and perfusion parameters in allografts to detect AR and differentiate among AR, IRI and CSA.

In conclusion, this study demonstrated the value of IVIM MRI for the detection of AR in rats; in particular, D* in the cortex and f in the medulla may be used to differentiate AR from IRI and CSA. Moreover, this study confirmed the value of BOLD MRI in differentiating among AR, IRI and CSA. Furthermore, the impairment of diffusion, perfusion and oxygen consumption were closely related to renal damage at histology. Thus, fMRI with IVIM and BOLD allows longitudinal assessment of renal allograft pathophysiology and might facilitate monitoring the effect of transplant immunosuppression.

Acknowledgment

We thank Yang Liu and Ying Wang for the assistance in pathological work.

Funding

This work was supported by the National Natural Science Foundation of China [grant numbers 81670679].

Declarations of interest

None.

References

[1] Nankivell BJ, Alexander SI. Rejection of the kidney allograft. N Engl J Med 2010;363(15):1451–62.
[2] Zhang JL, Rusinek H, Chandarana H, Lee VS. Functional MRI of the kidneys. J Magn Reson Imaging 2013;37(2):282–93.
[3] Park SY, Kim CK, Park BK, Kim SJ, Lee S, Huh W. Assessment of early renal allograft dysfunction with blood oxygenation level-dependent MRI and diffusion-weighted imaging. Eur J Radiol 2014;83(12):2114–21.
[4] Hueper K, Khalifa AA, Brasen JH, Vo Chieu VD, Gutberlet M, Wintterle S, et al. Diffusion-weighted imaging and diffusion tensor imaging detect delayed graft function and correlate with allograft fibrosis in patients early after kidney transplantation. J Magn Reson Imaging 2016;44(1):112–21.
[5] Hueper K, Hensen B, Gutberlet M, Chen R, Hartung D, Barrmeyer A, et al. Kidney transplantation: multiparametric functional magnetic resonance imaging for assessment of renal allograft pathophysiology in mice. Investig Radiol 2016;51(1):58–65.
[6] Giannarini G, Petralia G, Thoeny HC. Potential and limitations of diffusion-weighted magnetic resonance imaging in kidney, prostate, and bladder cancer including pelvic lymph node staging: a critical analysis of the literature. Eur Urol 2012;61(2):326–40.
[7] Kone BC. A 'BOLD' new approach to renal oxygen economy. Circulation 1996;94(12):3067–8.
[8] Le Bihan D, Breton E, Lallemand D, Aubin ML, Vignaud J, Laval-Jeantet M. Separation of diffusion and perfusion in intravoxel incoherent motion MR imaging. Radiology 1988;168(2):497–505.
[9] Lee S. An improved technique of renal transplantation in the rat. Surgery 1967;61(5):771–3.
[10] Hu X, Okabayashi T, Cameron AM, Wang Y, Hisada M, Li J, et al. Chimeric allografts induced by short-term treatment with stem cell-mobilizing agents result in long-term kidney transplant survival without immunosuppression: a study in rats. Am J Transplant 2016;16(7):2055–65.
[11] Grabner A, Kentrup D, Pawelski H, Muhlmeister M, Biermann C, Edemir B, et al. Renal contrast-enhanced sonography findings in a model of acute cellular allograft rejection. Am J Transplant 2016;16(5):1612–9.
[12] Reuter S, Schnockel U, Schroter R, Schober O, Pavenstadt H, Schafers M, et al. Non-invasive imaging of acute renal allograft rejection in rats using small animal F-FDG-PET. PLoS One 2009;4(4):e5296.
[13] Zakrzewicz A, Krasteva G, Wilhelm J, Dietrich H, Wilker S, Padberg W, et al. Reduced expression of arrestin beta 2 by graft monocytes during acute rejection of rat kidneys. Immunobiology 2011;216(7):854–61.
[14] Haas M, Sis B, Racusen LC, Solez K, Glotz D, Colvin RB, et al. Banff 2013 meeting report: inclusion of c4d-negative antibody-mediated rejection and antibody-associated arterial lesions. Am J Transplant 2014;14(2):272–83.
[15] Feige JN, Sage D, Wahli W, Desvergne B, Gelman L. PixFRET, an ImageJ plug-in for FRET calculation that can accommodate variations in spectral bleed-throughs. Microsc Res Tech 2005;68(1):51–8.
[16] Liang L, Chen WB, Chan KW, Li YG, Zhang B, Liang CH, et al. Using intravoxel incoherent motion MR imaging to study the renal pathophysiological process of contrast-induced acute kidney injury in rats: comparison with conventional DWI and arterial spin labelling. Eur Radiol 2016;26(6):1597–605.
[17] Thoeny HC, Zumstein D, Simon-Zoula S, Eisenberger U, De Keyzer F, Hofmann L, et al. Functional evaluation of transplanted kidneys with diffusion-weighted and BOLD MR imaging: initial experience. Radiology 2006;241(3):812–21.
[18] Notohamiprodjo M, Kalnins A, Andrassy M, Kolb M, Ehle B, Mueller S, et al. Multiparametric functional MRI: a tool to uncover subtle changes following allogeneic renal transplantation. PLoS One 2016;11(11):e0165532.
[19] Hueper K, Gutberlet M, Brasen JH, Jang MS, Thorenz A, Chen R, et al. Multiparametric functional MRI: non-invasive imaging of inflammation and edema formation after kidney transplantation in mice. PLoS One 2016;11(9):e0162705.
[20] Chandarana H, Kang SK, Wong S, Rusinek H, Zhang JL, Arizono S, et al. Diffusion-weighted intravoxel incoherent motion imaging of renal tumors with histopathologic correlation. Investig Radiol 2012;47(12):688–96.
[21] Sigmund EE, Vivier PH, Sui D, Lamparello NA, Tantillo K, Mikheev A, et al. Intravoxel incoherent motion and diffusion-tensor imaging in renal tissue under hydration and furosemide flow challenges. Radiology 2012;263(3):758–69.
[22] Aktas A. Transplanted kidney function evaluation. Semin Nucl Med 2014;44(2):129–45.
[23] Farina R, Pennisi F, La Rosa M, Puglisi C, Di Benedetto A, Campisi G, et al. Functional study of the transplanted kidney with power Doppler US and time/intensity curves. Radiol Med 2007;112(1):64–73.
[24] Sadowski EA, Fain SB, Alford SK, Korosec FR, Fine J, Muehrer R, et al. Assessment of acute renal transplant rejection with blood oxygen level-dependent MR imaging: initial experience. Radiology 2005;236(3):911–9.
[25] Hueper K, Schmidbauer M, Thorenz A, Brasen JH, Gutberlet M, Mengel M, et al. Longitudinal evaluation of perfusion changes in acute and chronic renal allograft rejection using arterial spin labeling in translational mouse models. J Magn Reson Imaging 2017;46(6):1664–72.
[26] Sadowski EA, Djamali A, Wentland AL, Muehrer R, Becker BN, Grist TM, et al. Blood oxygen level-dependent and perfusion magnetic resonance imaging: detecting differences in oxygen bioavailability and blood flow in transplanted kidneys. Magn Reson Imaging 2010;28(1):56–64.
[27] Kentrup D, Bovenkamp P, Busch A, Schuette-Nuetgen K, Pawelski H, Pavenstadt H, et al. GlucoCEST magnetic resonance imaging in vivo may be diagnostic of acute renal allograft rejection. Kidney Int 2017;92(3):757–64.
[28] Liu J, Han Z, Chen G, Li Y, Zhang J, Xu J, et al. CEST MRI of sepsis-induced acute kidney injury. NMR Biomed 2018;31(8):e3942.